Dynamic analysis of flexoelectric systems in the frequency domain with isogeometric analysis

Xing Chen, Song Yao, Julien Yvonnet

Computational Mechanics manuscript No.
(will be inserted by the editor)

Dynamic analysis of flexoelectric systems in the frequency domain with Isogeometric Analysis

Xing Chen[1,2], **Song Yao**[1], **Julien Yvonnet**[2⋆]

[1] Key Laboratory of Traffic Safety on Track, Ministry of Education, School of Traffic & Transportation Engineering, Central South University, Changsha 410075, China

[2] Université Gustave Eiffel, CNRS, MSME UMR 8208, F-77454 Marne-la-Vallée, France

Received: date / Revised version: date

Abstract A numerical procedure based on Isogeometric Analysis (IGA) is developed to analyze the dynamic response of flexoelectric systems in the frequency domain. In materials or composites with an effective flexoelectric response, a polarization can be induced by local strain gradients. In general, these effects are small in the static regime. However, larger effects may be induced by dynamic loads, and can be used in energy harvesters converting mechanical vibrations into electrical energy. In this work, the equations describing frequency response of flexoelectric systems under dynamic loads are first described. Then, an IGA discretization procedure is employed to handle the C^1 continuity of the displacement fields. The conditions of both open and close-circuits are formulated. The numer-

Send offprint requests to:

⋆ *Present address:* julien.yvonnet@univ-eiffel.fr

ical methodology is used to evaluate the sensitivity of different parameters such as load resistors, dynamic scale parameter, and the use of flexoelectric or non-flexoelectric materials on the frequency response of output voltage, power and displacements of beam-like structures, possibly incorporating structural geometrical features. The potential of IGA with respect to mesh refinement (h-refinement) and higher order approximation (p-refinement) for modeling complex geometries within the present framework is invetigated.

1 Introduction

Flexoelectricity describes the coupled electromechanical behavior when an electrical polarization is induced by a strain gradient (direct flexoelectricity), or when a mechanical strain is induced by a polarization gradient (converse flexoelectricity) in dielectric materials. With the miniaturization of electronic devices, flexoelectric effect have gained increasing attention as the effects are more pronounced when the size of the devices decreases. A wide range of promising application for flexoelectricity were studied, such as nano generators [1], energy harvesters [2,3], sensors and actuators [4,5]. Flexoelectric effect was first theoretically predicted by Mashkevich and Tolpygo [6], and experimentally observed in the 1960s [7]. However, a pioneering experimental measurement of flexoelectric coefficients was performed in the 2000s by Ma and Cross [8,9]. In [10], Kogan estimated the range of flexoelectric coefficients for several materials. The fourth-order partial differential equations for flexoelectricity in solid were solved with analytical methods on simple geometries in [11–14].

In general, flexoelectric effects are small in the static regime. However, larger effects may be induced by dynamic loads, and can be used in energy harvesters converting mechanical vibrations into electrical energy. The analytic solutions of flexoelectric dynamic models have been obtained in several studies focusing on simple Euler-Bernoulli or Timoshenko beams. Deng examined the output power density and conversion efficiency of flexoelectric energy harvesters [2], and studied the impact of the flexo-dynamic effects on nanoscale energy harvesters [15]. Baroudi [16] analyzed analytically the static and dynamic responses of nanobeam with different boundary conditions. Wang[17] developed an analytical model incorporating flexoelectric effects for nanoscale unimorph piezoelectric energy harvesters with arbitrary length and position of piezoelectric layer and proof mass. Flexoelectric vibrating models can be used as sensors [18], actuators and vibration control of flexoelectric beam [19,20]. The surface and size effects were introduced to the dynamic response of flexoelectric energy harvesters in [21] and in nanobeams in [22,23]. Nguyen [24] investigated the influence of dynamic flexoelectric effect on the natural frequency of both the Timoshenko and Euler-Bernoulli beams, where the flexo-dynamic term and dynamic polarization were both considered. Yu [25] studied dynamic flexoelectric effects in functionally graded piezoelectric nano beams. The dynamic responses of nanoplates with flexoelectric effect in Kirchhoff plates was proposed by [26,27]. Other studies incorporating nonlinear effects in dynamic response of flexoelectric systems can be found in [28–32].

For general geometries, the main difficulty is due to the fourth-order nature of the flexoelectric partial differential equation, requiring C^1 continuity of the dis-

cretized displacement field. Several numerical methods were proposed to solve this issue, including the local maximum-entropy (LME) meshfree methods [33, 34], mixed FEM [35, 36], isogeometric analysis [37–39], B-spline techniques [40], or the Argyris triangular elements [41]. Several numerical methodologies for dynamic analysis of flexoelectric models were proposed. Kumar developed a finite element analysis of flexoelectric energy harvester where a trapezoidal shaped cantilever was optimized for a wide range of excitation frequencies [42], and used it on a flexoelectric bi-stable energy harvester [43]. Thai [44] developed a staggered explicit-implicit isogeometric formulation for large deformation flexoelectricity based on transient analysis. Xue [45] presented a flexoelectric micro cantilever energy harvester with a broad bandwidth. A few papers incorporated strain gradient inertial effects in the formulation (see [46–49]). A review paper summarizing the different dynamic flexoelectric formulations can be found in [50].

In this work, we developed an isogeometric analysis (IGA) framework to solve the dynamic response of flexoelectric energy harvesters for arbitrary geometries, in the frequency domain, including strain gradient inertial effects. Note that we do not consider here flexoelectric dynamic effects related to the coupling between velocity and rate of polarization, which could be investigated in future studies. As compared to the previous related works available in the literature, the IGA discretization is proposed here for the first time to solve dynamic flexoelectric problems in the frequency domain. The conditions of both open and close-circuits are formulated. The numerical methodology is used to evaluate the sensitivity of different parameters such as load resistors, flexoelectric coefficients and dynamic

scale parameter on the frequency response of output voltage, power and displacements of a beam-like structure with structural geometrical features, to evaluate the potential of the proposed IGA approach, and its advantages for $h-$ and $p-$ refinements when considering complex geometries.

2 Static flexoelectricity

The equations governing the static flexoelectric equilibrium are first reviewed. An open domain $\Omega \subset \mathbb{R}^2$ is considered, with boundary $\partial\Omega$. The boundary is composed of Dirichlet and Neumann parts, which are denoted by $\partial\Omega_u$ and $\partial\Omega_t$ for the displacement problem, respectively, and $\partial\Omega_\phi$ and $\partial\Omega_D$ for the electric problem, respectively, such as $\partial\Omega_u \cup \Omega_t = \partial\Omega$, $\partial\Omega_u \cap \Omega_t = \emptyset$ and $\partial\Omega_\phi \cup \Omega_D = \partial\Omega$, $\partial\Omega_\phi \cap \Omega_D = \emptyset$. In the following, bold symbols denote vectors or tensors, while non-bold symbols denote scalars or tensor components.

The electric enthalpy density h^* of a linear electromechanical system, where piezoelectricity and flexoelectricity are both taken into account, is expressed by [2, 33,49]:

$$h^* = \frac{1}{2}C_{ijkl}\varepsilon_{ij}\varepsilon_{kl} - \frac{1}{2}\alpha_{ij}E_iE_j - e_{ijk}E_k\varepsilon_{ij} - \mu_{ijkl}E_i\nabla\varepsilon_{jkl} + \frac{1}{2}G_{ijklmn}\nabla\varepsilon_{ijk}\nabla\varepsilon_{lmn} \tag{1}$$

In Eq. (1), $\mathbf{C}$, $\boldsymbol{\alpha}$ and $\mathbf{e}$ denote the fourth-order elastic, second-order dielectric and third-order piezoelectric tensors, respectively, $\boldsymbol{\mu}$ denotes the fourth-order flexoelectric tensor, while $\mathbf{G}$ is the sixth-order strain gradient elastic tensor. Note that the above model does not include converse flexoelectric effects [51]. For further extensions about this model, see e.g. [52].

The strain tensor ε, the strain-gradient tensor $\nabla\varepsilon$ and the electric field vector $\mathbf{E}$ are related to displacement vector $\mathbf{u}$ and the electric potential ϕ through:

$$\varepsilon_{ij} = \frac{1}{2}(u_{i,j} + u_{j,i}) \tag{2}$$

$$E_i = -\phi_{,i} \tag{3}$$

$$\nabla\varepsilon_{ijk} = \varepsilon_{ij,k} = \frac{1}{2}(u_{i,jk} + u_{j,ik}) \tag{4}$$

Then the constitutive equations are obtained by:

$$\sigma_{ij} = \frac{\partial h^*}{\partial \varepsilon_{ij}} = C_{ijkl}\varepsilon_{kl} - e_{kij}E_k \tag{5}$$

$$d_i = -\frac{\partial h^*}{\partial E_i} = \alpha_{ij}E_j + e_{ijk}\varepsilon_{jk} + \mu_{ijkl}\nabla\varepsilon_{jkl} \tag{6}$$

$$\tau_{ijk} = \frac{\partial h^*}{\partial \nabla\varepsilon_{ijk}} = G_{ijklmn}\nabla\varepsilon_{lmn} - \mu_{ijkl}E_l \tag{7}$$

where the $\boldsymbol{\sigma}$, $\mathbf{d}$ and $\boldsymbol{\tau}$ denote stress, electric displacement and hyperstress tensors, respectively. The equations of the dielectric problem without free charge and mechanical problem without body force are given by [12]

$$d_{i,i} = 0 \text{ in } \Omega \tag{8}$$

$$\sigma_{ij,j} - \tau_{ijk,jk} \text{ in } \Omega \tag{9}$$

The problem is completed by boundary conditions for the electric problem as

$$\phi = \phi^d \text{ on } \partial\Omega_\phi \tag{10}$$

$$d_i n_i = -D_n^d \text{ on } \partial\Omega_D \tag{11}$$

where ϕ^d and D_n^d are the prescribed electric potential and surface charge density and $\mathbf{n}$ is the unitary normal vector to the boundary $\partial\Omega$. The mechanical boundary

conditions are given by (see e.g. [33]):

$$u_i = u_i^d \text{ on } \partial\Omega_u \tag{12}$$

$$t_k = n_j\left(\sigma_{jk} - \tau_{ijk,i}\right) - D_j\left(n_i\tau_{ijk}\right) = F_k^d \text{ on } \partial\Omega_F \tag{13}$$

where $\mathbf{u}^d$ and $\mathbf{F}^d$ are the prescribed mechanical displacements and tractions, and $D_j(.) = \frac{\partial(.)}{\partial x_j} - n_j n_q \frac{\partial(.)}{\partial x_q}$. Due to strain gradients, additional boundary conditions are considered:

$$u_{i,j}n_j = v_i^d \text{ on } \partial\Omega_v \tag{14}$$

$$n_i n_j \tau_{ijk} = r_k^d \text{ on } \partial\Omega_r \tag{15}$$

with $\partial\Omega_v \cup \Omega_r = \partial\Omega$, $\partial\Omega_v \cap \Omega_r = \emptyset$. Here, we assume natural boundary conditions on $\partial\Omega_v$ and Ω_r, i.e. $\mathbf{v}^d = \mathbf{r}^d = 0$.

3 Dynamic flexoelectricity

The total electric enthalpy H, the kinetic energy K, the Rayleigh dissipation $\tilde{R}$ and the external work W^{ext} are expressed by [33,50] :

$$H = \int_\Omega h^* d\Omega \tag{16}$$

$$K = \int_\Omega \frac{1}{2}\rho\dot{u}_i\dot{u}_i + \frac{1}{2}\ell_d^2\dot{u}_{i,j}\dot{u}_{i,j}d\Omega \tag{17}$$

$$\tilde{R} = \int_{\Omega} \frac{1}{2} V_{ij} \dot{u}_i \dot{u}_i d\Omega \tag{18}$$

$$W^{ext} = \int_{\partial\Omega_t} F_i^d u_i dS - \int_{\partial\Omega_D} D_n^d \phi dS \tag{19}$$

Above, ρ is the density, $\dot{(.)}$ indicates time derivative, ℓ_d is dynamic scaling parameter (micro inertia characteristic length). The term $\ell_d^2 \dot{u}_{i,j} \dot{u}_{i,j}$ is a dynamic term associated with the strain gradient problem [50,53] and $\mathbf{V}$ denotes viscous damping coefficients. Let us group all unknown quantities, respectively the displacement vector $\mathbf{u}$ and the potential ϕ in a vector $\mathbf{q}$. From the Hamilton's principle, the following Lagrangian equations are obtained, taking into account dissipation due to viscous damping terms:

$$\frac{d}{dt}\left(D_{\delta\dot{\mathbf{q}}} L\right) - D_{\delta\mathbf{q}} L + D_{\delta\dot{\mathbf{q}}} R = W^{ext} \tag{20}$$

where $D_{\delta\mathbf{v}} f(\mathbf{u})$ is the directional derivative, expressed by

$$D_{\delta\mathbf{v}} f(\mathbf{u}) = \left[\frac{df(\mathbf{u} + \alpha\delta\mathbf{v})}{d\alpha}\right]_{\alpha=0} \tag{21}$$

and $D_{\mathbf{q}} = D_{\delta\mathbf{u}} + D_{\delta\phi}$, $D_{\dot{\mathbf{q}}} = D_{\dot{\delta}\mathbf{u}}$ and

$$L = K - H \tag{22}$$

We have, using (17):

$$D_{\dot{\mathbf{q}}}L = D_{\dot{\mathbf{u}}}L = \int_{\Omega} D_{\dot{\mathbf{u}}}K d\Omega = \int_{\Omega} \rho \dot{u}_i \delta \dot{u}_i + \ell_d^2 \dot{u}_{i,j} \delta \dot{u}_{i,j} d\Omega \tag{23}$$

Then,

$$\frac{d}{dt}\left(D_{\dot{\mathbf{q}}}L\right) = \int_{\Omega} \rho \ddot{u}_i \delta \dot{u}_i + \ell_d^2 \ddot{u}_{i,j} \delta \dot{u}_{i,j} d\Omega \tag{24}$$

and

$$D_{\delta L} = -D_{\delta \mathbf{u}}H - D_{\delta \phi}H d\Omega \quad . \tag{25}$$

We have, using (1)-(16):

$$D_{\delta \mathbf{u}}H = \int_{\Omega} C_{ijkl}\varepsilon_{ij}\delta\varepsilon_{kl} - e_{ijk}\delta\varepsilon_{ij}E_k - \mu_{ijkl}E_i\delta\nabla\varepsilon_{jkl} + G_{ijklmn}\nabla\varepsilon_{ijk}\delta\nabla\varepsilon_{lmn}d\Omega \tag{26}$$

$$D_{\delta \phi}H = \int_{\Omega} \alpha_{ij}E_i\delta\phi_{,j} + e_{ijk}\varepsilon_{ij}\delta\phi_{,k} + \mu_{ijkl}\delta\phi_{,i}\nabla\varepsilon_{jkl}d\Omega \tag{27}$$

and

$$D_{\delta \dot{\mathbf{q}}}\tilde{R} = D_{\delta \dot{\mathbf{u}}}\tilde{R} = \int_{\Omega} V_{ij}\dot{u}_i\delta u_j d\Omega \tag{28}$$

We finally obtain the weak forms:

$$\int_{\Omega} \sigma_{ij}\delta\varepsilon_{ij} + \tau_{ijk}\delta\nabla\varepsilon_{ijk} + \rho\ddot{u}_i\delta u_i + \ell_d^2\ddot{u}_{i,j}\delta u_{i,j} + V_{ij}\dot{u}_i\delta u_j d\Omega = \int_{\partial\Omega_t} F_i^d \delta u_i dS \tag{29}$$

$$\int_{\Omega} d_i\delta\phi_{,i}d\Omega = \int_{\partial\Omega_D} D_n^d\delta\phi dS \tag{30}$$

with $\delta\varepsilon_{ij} = \frac{1}{2}\left(\delta u_{i,j} + \delta u_{j,i}\right)$ and $\delta\nabla\varepsilon_{ijk} = \frac{1}{2}\left(\delta u_{i,jk} + \delta u_{j,ik}\right)$.

4 IGA discretization of dynamic flexoelectricity equations

4.1 IGA discretization scheme

The flexoeoectric problem requires at least C^1 continuity of displacement fields due to the strain gradient terms in (29). Different approaches have been proposed in the literature, as described in the introduction. In this work, we use Isogeometric Analysis (IGA) [54] for the discretization of the dynamic flexoelectric problem in the frequency domain. In isogeometric analysis, the NURBS (Non-Uniform Rational B-Spline) are used to construct curves, surface and solid, and NURBS basis functions are employed to approximate the physical fields like the displacements (see e.g. [54,55]). The NURBS basis functions are defined by

$$R_{i,p}(\xi) = \frac{N_{i,p}(\xi)w_i}{W(\xi)} = \frac{N_{i,p}(\xi)w_i}{\sum_{j=1}^{n} N_{j,p}(\xi)w_j} \tag{31}$$

where $\boldsymbol{\xi} = \{\xi_1, \xi_2, ..., \xi_{n+p+1}\}$, denote the knots, p is the polynomial order, n is the number of basis function and $w_i,\ i = 1,2,...,n$ are positive weights. It is worth noting that when all the weights are equal, the NURBS basis degenerate to the B-Spline basis. In (31), $N_{i,p}(\xi)$ are B-Spline basis functions which are recursively defined using the Cox-de Boor formula [56] and starting with piecewise constants functions ($p = 0$):

$$N_{i,0} = \begin{cases} 0, \; if \; \xi_i \leq \xi \leq \xi_{i+1} \\ 1, \quad \text{otherwise.} \end{cases} \tag{32}$$

For $p = 1, 2, ...$, we have

$$N_{i,p}(\xi) = \frac{\xi - \xi_i}{\xi_{i+p} - \xi_i} N_{i,p-1}(\xi) + \frac{\xi_{i+p+1} - \xi}{\xi_{i+p+1} - \xi_{i+1}} N_{i+1,p-1}(\xi) \tag{33}$$

The NURBS surfaces are formulated as

$$S(\xi, \eta) = \sum_{i=1}^{n} \sum_{j=1}^{m} R_{i,j}^{p,q}(\xi, \eta) \mathbf{B}_{i,j} \tag{34}$$

Where $\mathbf{B}_{i,j}$ are the coordinates of the control points. The rational terms $R_{i,j}^{p,q}$ are provided by

$$R_{i,j}^{p,q}(\xi, \eta) = \frac{N_i(\xi) M_j(\eta) w_{i,j}}{\sum_{\hat{i}=1}^{n} \sum_{\hat{j}=1}^{m} N_{\hat{i},p}(\xi) M_{\hat{j},q}(\eta) w_{\hat{i},\hat{j}}} \tag{35}$$

and $N_{i,p}(\xi)$ and $M_{i,q}(\eta)$ are univariate B-Spline basis of order p and q corresponding to knot vectors $\boldsymbol{\xi}$ and $\boldsymbol{\eta}$, respectively.

In this work, the IGA discretization for the problem defined in (29)-(30) is presented with 2D plane strain assumption. The displacement $\mathbf{u}$ and electric potential ϕ fields are both approximated using NURBS according to

$$\mathbf{u}(\mathbf{x}) = \sum_{i=1}^{n} \sum_{j=1}^{m} R_{i,j}^{p,q}(\xi, \eta) u_{ij}^{e} = \boldsymbol{N}_u \boldsymbol{u}^e \tag{36}$$

$$\phi(\mathbf{x}) = \sum_{i=1}^{n} \sum_{j=1}^{m} R_{i,j}^{p,q}(\xi, \eta) \phi^e = \boldsymbol{N}_\phi \boldsymbol{\phi}^e \tag{37}$$

defining the following vectors:

$$\mathbf{u}^e = \left[u_x^1, u_x^2, ..., u_x^n, u_y^1, u_y^2, ..., u_y^n \right] \tag{38}$$

$$\phi^e = \left[\phi^1, \phi^2, ..., \phi^n\right] \tag{39}$$

$$[\varepsilon] = [\varepsilon_{11}, \varepsilon_{22}, 2\varepsilon_{12}] \tag{40}$$

$$[\nabla\varepsilon] = [\nabla\varepsilon_{111}, \nabla\varepsilon_{221}, 2\nabla\varepsilon_{122}, \nabla\varepsilon_{222}, 2\nabla\varepsilon_{121}] \tag{41}$$

and the different following quantities are obtained from the shape function derivatives by

$$[\varepsilon] = \boldsymbol{B}_u \boldsymbol{u}^e \tag{42}$$

$$\boldsymbol{E} = -\boldsymbol{B}_\phi \phi^e \tag{43}$$

$$[\nabla\varepsilon] = \boldsymbol{H}_u \boldsymbol{u}^e \tag{44}$$

where $\mathbf{B}_u$, $\mathbf{B}_\phi$ and $\mathbf{H}_u$ are shape function derivative matrices, given by

$$\boldsymbol{B}_\phi = \begin{bmatrix} \frac{\partial N_1}{\partial x} & \cdots & \frac{\partial N_n}{\partial x} \\ \frac{\partial N_1}{\partial y} & \cdots & \frac{\partial N_n}{\partial y} \end{bmatrix}, \; \boldsymbol{B}_u = \begin{bmatrix} \frac{\partial N_1}{\partial x} & \cdots & \frac{\partial N_n}{\partial x} & 0 & \cdots, & 0 \\ 0 & \cdots & 0 & \frac{\partial N_1}{\partial y} & \cdots & \frac{\partial N_n}{\partial y} \\ \frac{\partial N_1}{\partial y} & \cdots & \frac{\partial N_n}{\partial y} & \frac{\partial N_1}{\partial x} & \cdots & \frac{\partial N_n}{\partial x} \end{bmatrix} \tag{45}$$

$$\boldsymbol{H}_u = \begin{bmatrix} \frac{\partial^2 N_1}{\partial x^2} & \cdots & \frac{\partial^2 N_n}{\partial x^2} & 0 & \cdots & 0 \\ 0 & \cdots & 0 & \frac{\partial^2 N_1}{\partial x \partial y} & \cdots & \frac{\partial^2 N_n}{\partial x \partial y} \\ \frac{\partial^2 N_1}{\partial y^2} & \cdots & \frac{\partial^2 N_n}{\partial y^2} & \frac{\partial^2 N_1}{\partial x \partial y} & \cdots & \frac{\partial^2 N_n}{\partial x \partial y} \\ 0 & \cdots & 0 & \frac{\partial^2 N_1}{\partial y^2} & \cdots & \frac{\partial^2 N_n}{\partial y^2} \\ \frac{\partial^2 N_1}{\partial x \partial y} & \cdots & \frac{\partial^2 N_n}{\partial x \partial y} & 0 & \cdots & 0 \\ \frac{\partial^2 N_1}{\partial x \partial y} & \cdots & \frac{\partial^2 N_n}{\partial x \partial y} & \frac{\partial^2 N_1}{\partial x^2} & \cdots & \frac{\partial^2 N_n}{\partial x^2} \end{bmatrix} \tag{46}$$

and $\mathbf{u}^e$ and ϕ^e denote the nodal displacements and potentials, respectively.

When only static equilibrium is considered, substituting (36)-(44) into (29)-(30) yields a discrete system of algebraic equations in the form:

$$\begin{bmatrix} \mathbf{K}_{uu} & \mathbf{K}_{u\phi} \\ -\mathbf{K}_{u\phi}^T & \mathbf{K}_{\phi\phi} \end{bmatrix} \begin{bmatrix} \mathbf{u} \\ \phi \end{bmatrix} = \begin{bmatrix} \mathbf{f}_u \\ \mathbf{f}_\phi \end{bmatrix} \tag{47}$$

with

$$\mathbf{K}_{uu} = \int_\Omega [\boldsymbol{B}_u^T \mathbf{C} \boldsymbol{B}_u + \boldsymbol{H}_u^T \mathbf{G} \boldsymbol{H}_u] d\Omega \tag{48}$$

$$\mathbf{K}_{u\phi} = \int_\Omega [\boldsymbol{B}_\phi^T \mathbf{e} \boldsymbol{B}_u + \boldsymbol{B}_\phi^T \boldsymbol{\mu} \boldsymbol{H}_u] d\Omega \tag{49}$$

$$\mathbf{K}_{\phi\phi} = \int_\Omega [\boldsymbol{B}_\phi^T \boldsymbol{\alpha} \boldsymbol{B}_\phi] d\Omega \tag{50}$$

$$\mathbf{f}_u = \int_\Omega \mathbf{N}_u^T \mathbf{F}^d d\Omega \tag{51}$$

$$\mathbf{f}_\phi = -\int_\Omega \mathbf{N}_\phi^T D_n^d d\Omega \tag{52}$$

Moreover, the material parameters $\mathbf{C}$, $\boldsymbol{e}$, $\boldsymbol{\alpha}$, $\boldsymbol{\mu}$ and $\mathbf{G}$ can be defined in the matrix form [34,57] as

$$\mathbf{C}=\begin{bmatrix} c_{11} & c_{12} & 0 \\ c_{12} & c_{22} & 0 \\ 0 & 0 & c_{44} \end{bmatrix},\quad \boldsymbol{e}=\begin{bmatrix} e_{111} & e_{122} & e_{112} \\ e_{211} & e_{222} & e_{212} \end{bmatrix},\quad \boldsymbol{\alpha}=\begin{bmatrix} \alpha_{11} & 0 \\ 0 & \alpha_{33} \end{bmatrix} \tag{53}$$

$$\boldsymbol{\mu}=\begin{bmatrix} \mu_{1111} & \mu_{1221} & \mu_{1122} & \mu_{1222} & \mu_{1112} & \mu_{1121} \\ \mu_{2111} & \mu_{2221} & \mu_{2122} & \mu_{2222} & \mu_{2112} & \mu_{2121} \end{bmatrix} \tag{54}$$

For the sake of simplicity, we assume the matrix $\mathbf{G}$ is in the form:

$$\mathbf{G}=\ell^2\begin{bmatrix} c_{11} & 0 & 0 & c_{12} & 0 & 0 \\ 0 & c_{11} & c_{12} & 0 & 0 & 0 \\ 0 & c_{12} & c_{11} & 0 & 0 & 0 \\ c_{12} & 0 & 0 & c_{11} & 0 & 0 \\ 0 & 0 & 0 & 0 & c_{44} & 0 \\ 0 & 0 & 0 & 0 & 0 & c_{44} \end{bmatrix} \tag{55}$$

4.2 IGA discretization of dynamic flexoelectricity in the frequency domain

When dynamic terms are taken into account, introducing (36)-(44) into (29)-(30) yields the following discrete set of time-differential equations:

$$\begin{cases} \mathbf{M}\ddot{\mathbf{u}}+\mathbf{D}\dot{\mathbf{u}}+\mathbf{K}_{uu}\mathbf{u}+\mathbf{K}_{u\phi}\boldsymbol{\phi}=\mathbf{f}_{\mathbf{u}} \\ -\mathbf{K}_{u\phi}^{T}\mathbf{u}+\mathbf{K}_{\phi\phi}\boldsymbol{\phi}=\mathbf{f}_{\phi} \end{cases} \tag{56}$$

where the mass matrix $\mathbf{M}$ and damping matrix $\mathbf{D}$ are defined by

$$\mathbf{M} = \int_{\Omega} \rho \{ \boldsymbol{N}_u^T \boldsymbol{N}_u + \ell_d^2 \tilde{\boldsymbol{B}}_u^T \tilde{\boldsymbol{B}}_u \} d\Omega \tag{57}$$

$$\mathbf{D} = \int_{\Omega} \mathbf{N}_u^T \mathbf{V} \mathbf{N} d\Omega \tag{58}$$

with

$$\tilde{\boldsymbol{B}}_u = \begin{bmatrix} \frac{\partial N_1}{\partial x} & \cdots & \frac{\partial N_n}{\partial x} & 0 & \cdots, & 0 \\ 0 & \cdots & 0 & \frac{\partial N_1}{\partial y} & \cdots & \frac{\partial N_n}{\partial y} \\ \frac{\partial N_1}{\partial y} & \cdots & \frac{\partial N_n}{\partial y} & 0 & \cdots & 0 \\ 0 & \cdots & 0 & \frac{\partial N_1}{\partial x} & \cdots & \frac{\partial N_n}{\partial x} \end{bmatrix} \tag{59}$$

Following classical approaches, the matrix $\mathbf{D}$ is approximated by

$$\mathbf{D} = \beta_1 \mathbf{M} + \beta_2 \mathbf{K}_{uu} \tag{60}$$

Above, β_1 and β_2 are constants computed by [2]:

$$\begin{bmatrix} \beta_1 \\ \beta_2 \end{bmatrix} = \frac{2\omega_1 \omega_2}{\omega_1^2 - \omega_2^2} \begin{bmatrix} -\omega_2 & \omega_1 \\ \frac{1}{\omega_2} & -\frac{1}{\omega_1} \end{bmatrix} \begin{bmatrix} \xi_1 \\ \xi_2 \end{bmatrix} \tag{61}$$

where ξ_1 and ξ_2 are two damping ratios, and ω_1 and ω_2 are the first two resonance frequencies of the structure.

The displacement field, the potential and the external forces are assumed to be in the form:

$$\mathbf{u} = \tilde{\mathbf{u}} e^{j\omega t},\ \phi = \tilde{\phi} e^{j\omega t},\ \mathbf{f_u} = \tilde{\mathbf{f}}_u e^{j\omega t} \tag{62}$$

where j is the complex number and ω is the frequency. In the case of an open circuit, $\mathbf{f}_\phi = \mathbf{0}$. Introducing (62) in (56), we obtain:

$$\begin{bmatrix} \left(\mathbf{K}_{uu} + j\omega\mathbf{D} - \omega^2\mathbf{M}\right) & \mathbf{K}_{u\phi} \\ -\mathbf{K}_{u\phi}^T & \mathbf{K}_{\phi\phi} \end{bmatrix} \begin{bmatrix} \tilde{\mathbf{u}} \\ \tilde{\phi} \end{bmatrix} = \begin{bmatrix} \tilde{\mathbf{f}}_u \\ \mathbf{0} \end{bmatrix} \tag{63}$$

In this work, boundary conditions associated with a close-circuit, as illustrated in Fig. 1(b), are considered. Following [58], we have:

$$\dot{\mathbf{f}}_\phi = \frac{\hat{\phi}}{R} \tag{64}$$

where R is the resistor value and $\hat{\phi}$ is the vector of nodal potentials where the resistor is connected. The vector $\hat{\phi}$ is related to the global unknown vector $\tilde{\phi}$ through a matrix $\mathbf{T}$ such that $\hat{\phi} = \mathbf{T}\tilde{\phi}$ and which contains mainly zeros and ones. Deriving the last equation of (56) with respect to time we obtain:

$$-\mathbf{K}_{u\phi}^T\dot{\mathbf{u}} + \mathbf{K}_{\phi\phi}\dot{\phi} = \dot{\mathbf{f}}_\phi \tag{65}$$

Then, using (62) and (64), it yields:

$$-j\omega\mathbf{K}_{u\phi}^T\tilde{\mathbf{u}} + j\omega\mathbf{K}_{\phi\phi}\tilde{\phi} = \frac{\hat{\phi}}{R} \tag{66}$$

The new linear system to be solved for a given frequency ω is given by:

$$\begin{bmatrix} \mathbf{K}_{uu} + j\omega\mathbf{D} - \omega^2\mathbf{M} & \mathbf{K}_{u\phi} \\ -\mathbf{K}_{u\phi}^T & \mathbf{K}_{\phi\phi} - \frac{\mathbf{T}}{j\omega R} \end{bmatrix} \begin{bmatrix} \tilde{\mathbf{u}} \\ \tilde{\phi} \end{bmatrix} = \begin{bmatrix} \tilde{\mathbf{f}}_u \\ \mathbf{0} \end{bmatrix} \tag{67}$$

5 Numerical examples

In this section, we first validate the present IGA formulation for dynamic flexoelectric calculations. Then, we use the present numerical model to discuss the influence of parameters in vibrating flexoelectric systems.

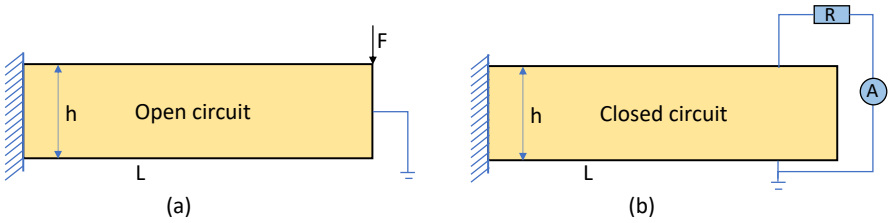

Fig. 1: Electromechanical coupling cantilever beam with (a) open circuit boundary conditions; (b) close-circuit boundary conditions.

5.1 Validation of the IGA flexoelectric model

5.1.1 Static flexoelectric benchmark First, we validate the present IGA framework on a static flexoelectric benchmark. A beam made of a flexoelectric material is considered, as shown in Fig. 1 (a). Displacements are fixed on the right-end, and a static force $F = 1$ N is prescribed on the top-right corner along the $y-$direction. On the left end, zero electric potential is prescribed to mimic an open circuit. The beam has dimensions $h \times L$. The length of the beam is $L = 20h$ and the thickness h varies. It is assumed that only the stress component σ_{11} and electric field component E_2 are non-zero. The analytical solution of the energy conversion d_{eff} for a 1-D flexoelectric beam model was provided in Majoub et al. [59] as:

$$d_{eff} = \frac{\chi}{1+\chi}\sqrt{\frac{\alpha}{Y}(e^2 + 12(\frac{\mu}{h}))} \tag{68}$$

where χ is electric susceptibility, $\alpha = \alpha_{33}$ is dielectric coefficient, Y is the Young's modulus, $e = e_{31}$ is the transversal piezoelectric coefficient, and $\mu = \mu_{12}$ is the transversal flexoelectric coefficient. Then the analytical expression of the normalized effective piezoelectric constant (NEPC) d^* for this problem was provided

as[59]

$$d^* = \frac{d_{eff}}{d_{piez}} = \sqrt{\left(1 + 12\left(\frac{\mu_{12}}{eh}\right)^2\right)} \tag{69}$$

To simulate the one-dimensional analytical model in [59], we simplify our model by neglecting the Poisson's ratio (i.e. $\nu = 0$) and considering only the transversal piezoelectric and flexoelectric constants e_{13} and μ_{12} to be non-zero. The numerical values of the coefficients are provided in Table 1. For numerical calculations, the rectangular domain corresponding to the beam is discretized with $N_x \times N_y$ B-spline elements of order 2. Considering plane strains, the matrices $\mathbf{K}_{\phi\phi}$ and $\mathbf{K}_{uu}$ in (47) are assembled using the values of $\mathbf{C}$, $\boldsymbol{\alpha}$, $\mathbf{e}$ in (53) as:

$$\mathbf{C} = \frac{Y}{(1+\nu)(1-2\nu)} \begin{bmatrix} 1-\nu & \nu & 0 \\ \nu & 1-\nu & 0 \\ 0 & 0 & \frac{1}{2}-\nu \end{bmatrix}, \ \boldsymbol{\alpha} = \begin{bmatrix} \alpha_{33} & 0 \\ 0 & \alpha_{33} \end{bmatrix} \tag{70}$$

$$\boldsymbol{\mu} = \begin{bmatrix} 0 & \mu_{12} & 0 & 0 & 0 & 0 \\ 0 & 0 & 0 & 0 & \mu_{12} & 0 \end{bmatrix} \quad \boldsymbol{e} = \begin{bmatrix} 0 & 0 & 0 \\ e_{31} & 0 & 0 \end{bmatrix} \tag{71}$$

and $\mathbf{G} = 0$ in (55). The NEPC is evaluated from the numerical IGA calculations by:

$$\tilde{d}^* = \frac{\sqrt{\frac{1}{2}\boldsymbol{\phi}_1 \cdot \mathbf{K}_{\phi\phi} \cdot \boldsymbol{\phi}_1}}{\sqrt{\frac{1}{2}\mathbf{u}_1 \cdot \mathbf{K}_{uu} \cdot \mathbf{u}_1}} \Bigg/ \sqrt{\frac{\frac{1}{2}\boldsymbol{\phi}_2 \cdot \mathbf{K}_{\phi\phi} \cdot \boldsymbol{\phi}_2}{\frac{1}{2}\mathbf{u}_2 \cdot \mathbf{K}_{uu} \cdot \mathbf{u}_2}} \tag{72}$$

where $\boldsymbol{\phi}$ and $\mathbf{u}$ are the vector solutions of the linear system (47), and the subscript 1 and 2 correspond to piezo-flexoelectric effects and only piezoelectric effects,

E	ν	μ_{12}	α_{33}	e_{31}
100 GPa	0	10 nC/m	$1nC/Vm$	-4.4 C/m^2

Table 1: Material parameters.

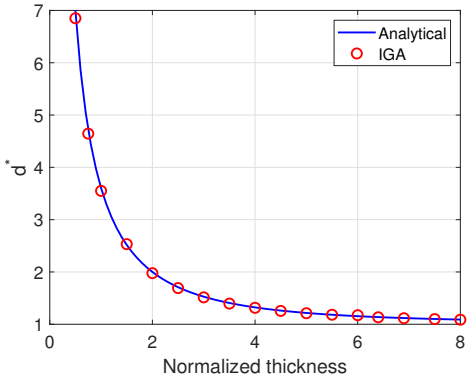

Fig. 2: Normalized effective piezoelectric coefficient (NEPC) with respect to normalized thickness h'.

respectively. A comparison between the analytical and the numerical NEPC solutions are provided in Fig. 2 for a fixed 240×24 B-Spline elements of order 2 and varying values of the normalized thickness $h' = -eh/\mu$. A very good agreement between both solutions can be appreciated.

5.1.2 Dynamic benchmark In this next example, we consider the free vibration of a cantilever beam with square section where the left end is fixed and the other boundaries are free. The objective is to validate the IGA scheme in the dynamic case. Here, the electromechanical coupling is not taken into account. The analyti-

cal expression of the natural frequencies f_r are given by [60]:

$$f_r = \frac{\lambda_r^2}{2\pi L^2}\sqrt{\frac{Eh^2}{12\rho}} \ \ (Hz) \tag{73}$$

where r is the frequency number, $I = bh^3/12$ ($b = h$ is width) is the moment of inertia for a square section, ρ is the density, and λ_r are the roots of the characteristic equation:

$$1 + \cos\lambda_r \cosh\lambda_r = 0 \tag{74}$$

Here, λ_1 is found numerically as $\lambda_1 = 1.875$. The other parameters are the same as in the previous example. The first natural frequency is computed from the IGA calculation by solving the eigenvalue problem

$$\mathbf{K}_{uu} - \omega_r^2 \mathbf{M} = 0, \ \ f_1 = \frac{\omega_1}{2\pi}. \tag{75}$$

A comparison between the present IGA and the exact solution is provided in Fig. 3, showing a very good agreement.

5.2 Frequency response of a flexoelectric beam

In this example, the effects of flexoelectricity on dynamic voltage, power and displacement responses of a beam are investigated. The voltage and displacement responses are defined as the absolute value of voltage and and displacement at the top right corner of the structure. The power is obtained as $P = \frac{\bar{\Phi}^2}{R}$, where $\bar{\Phi}$ is the potential at the top right corner of the structure. Both open and close-circuit

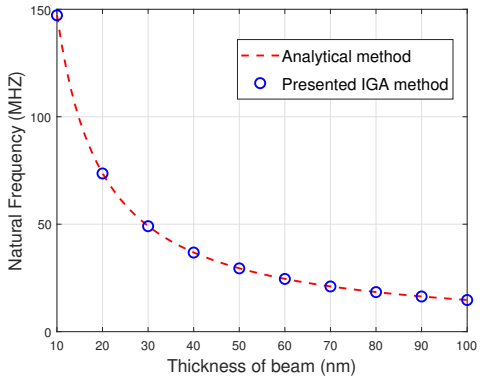

Fig. 3: Natural frequency of an elastic beam: comparison between exact and present IGA solutions.

boundary conditions, as depicted in Fig. 1 (a) and (b), are considered. The dimensions of the beam are $h = 200$ nm and $L = 2000$ nm. The left end is clamped and an excitation force $F(\omega) = F_y e^{j\omega t}$ is prescribed on the top right corner in the y-direction with F_y = 1 N. The effect of the resistor R is taken into account through Eq. (67). The material parameters of the material composing the beam are taken from [61] and correspond to a PZT/PZT composite. The corresponding coefficients are provided in Appendix 8. The density is taken as $\rho = 7500$ kg.m^{-3}. To define the matrix $\mathbf{G}$, we follow [62], and use the definition $G_{ijmkln} = C_{ijkl} L_{mn}$, where we use $L_{mn} = \ell \delta_{mn}$. There is no general agreement on the choice of the length scale ℓ. In [50], it is recommended that ℓ should be of the order of L, L being the typical characteristic length of heterogeneities. Then, we have chosen here $\ell = 10^{-8}$ m. Other authors have used such values, see e.g. [34]. In [50], Askes et al. suggested the heuristic rule for the dynamic length parameter $\ell_d > \ell$. In their work, they employed a gradient elasticity model to fit wave dispersion results of carbon

nanotubes based on molecular dynamics (MD) obtained by Wang et al. [63], and found a good agreement with the MD results when ℓ_d is in the range 3ℓ - 35ℓ. Then, in this work, ℓ_d was chosen as $\ell_d = 10\ell$. The modal damping ratios in (61) are found as $\xi_1 = \xi_2 = 0.01$. For the close-circuit of Fig. 1 (b), the potential on the top and bottom surfaces is enforced to be equal using a penalty method and the penalty parameter is taken as 10^2 (see e.g. [64]). The evolution of the voltage, $y-$displacement and power frequency responses are shown in Fig. 4, when the value of the resistor R varies. First, we can notice that the use of a flexoelectric material instead of a purely piezoelectric creates a voltage response while the purely piezoelectric material creates zero voltage (see Fig. 4). On the contrary, the displacement response is significantly larger when considering non-flexo material, and a small difference in the resonance frequency can be noticed. In Fig.4c, the amplitude of the output power decreases with respect to the increasing resistors, while the increase of output voltage is not significant.

In this last test, we evaluate the variation of the dynamic response of the system with respect to the dynamic length scale parameter ℓ_d, which is varied from 5ℓ to 30ℓ ($\ell = 10^{-8}$m). Results are presented in Fig. 5. We can note that changing ℓ_d has no influence on the amplitude of voltage and displacement reponses, and only small influence on the resonance frequency.

5.3 Dynamic behavior of a flexoelectric beam with periodic wavy shape

In this example, the dynamic response of a flexoelectric beamwith periodic wavy shape is investigated, to illustrate the present numerical framework for more com-

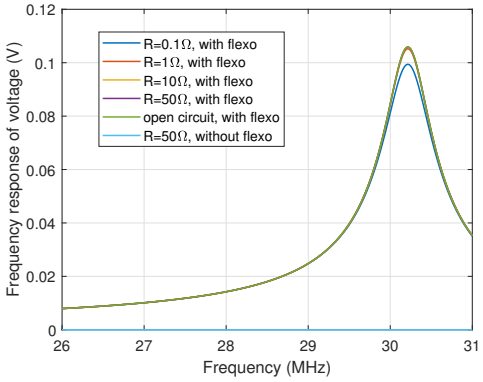

(a) Voltage frequency response

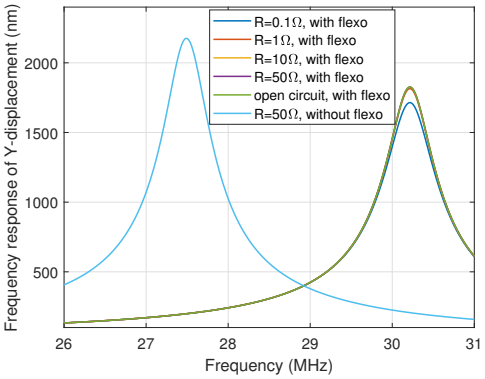

(b) y-displacement frequency response

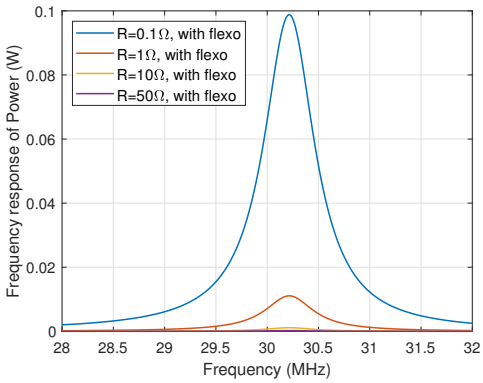

(c) Power frequency response

Fig. 4: (a) Voltage, (b) displacement and(c) power frequency responses for varying values of the resistor R in the open and close-circuit conditions.

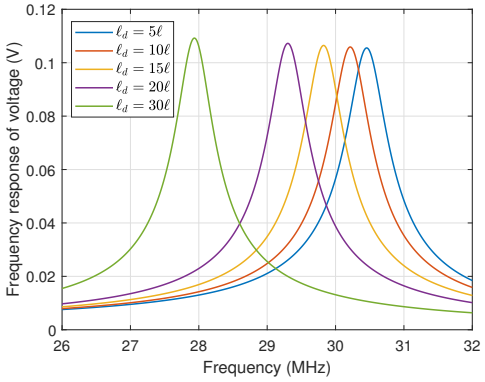

(a) Voltage frequency response

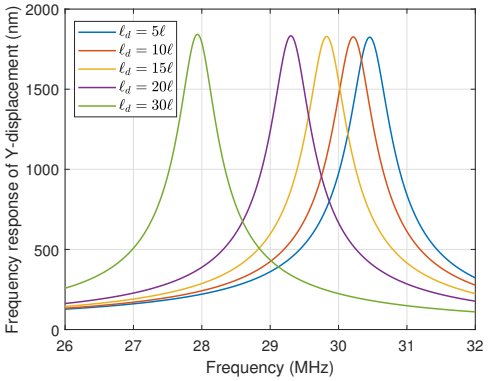

(b) y-displacement frequency response

Fig. 5: (a) Voltage and (b) displacement frequency responses for varying values of the micro inertial ℓ_d in the open circuit conditions.

plex structural geometries. The geometry of the beam is described in Fig. 6. The beam geometry is defined by 4×1 patterns of dimensions $H_1 \times H_2$= 200×300 nm^2 as described in Fig. 6 (b) and parametrized by a parameter h. The dimensions of the rectangular domain containing the patch are $H_1 = 200$ mm and $H_2 = 300$ mm. The geometric data, i.e. the coordinates of the control points defining the different

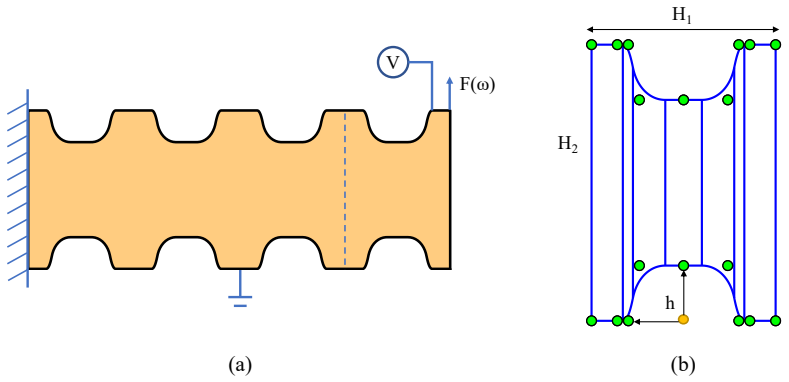

Fig. 6: Flexoelectric beam with periodic wavy shape: (a) geometry and boundary conditions; (b) initial IGA discretization of a periodic pattern.

NURBS curves of one cell, are provided in Table 2. Both open and closed circuit conditions are considered, but only the open circuit boundary conditions are depicted in Fig. 6. The closed circuit conditions are the same than in Fig. 1(b). The material parameters are the same than in the previous example and are provided in (76)-(80) while the dynamic length parameter is chosen as $\ell_d = 20\ell$.

First, the variations of voltage and y-displacements frequency responses are studied for a variation of h in the open-circuit conditions. Results are shown in Fig.7. It can be seen that a larger h increases displacement response while a small increase on voltage response, and with a significant decrease of the resonance frequency.

In Fig.8, voltage, $y-$displacement and power frequency responses are presented for the close-circuit, for different values of resistor R and fixed value of the parameter $h = 50$ nm. We can note that in this configuration, the voltage and dis-

i	$B_{i,1}(nm)$	$w_{i,1}$	$B_{i,2}(nm)$	$w_{i,2}$
1	(0,0)	1	(0 300)	1
2	(100-6h/5,0)	1	(100-6h/5,300)	1
3	(100-h,0)	1	(100-h,300)	1
4	(100-4h/5,h)	$\sqrt{2}/2$	(100-4h/5,300-h)	$\sqrt{2}/2$
5	(100,h)	1	(100,300-h)	1
6	(100+4h/5,h)	$\sqrt{2}/2$	(100+4h/5,300-h)	$\sqrt{2}/2$
7	(100+h,0)	1	(100+h,300)	1
8	(100+6h/5h,0)	1	(100+6h/5,300)	1
9	(200,0)	1	(200,300)	1

Table 2: Control points $B_{i,j}$ and weights $w_{i,j}$ for the geometry shown in Fig.6.

placement responses monotonically increase while increasing resistors decreases the power response. This suggests that an optimal resistor value must be chosen to maximize the effects in the application of flexoelectricity to energy harvesters.

The results associated with the same configuration but for the close-circuit with $R = 0.01\ \Omega$ are shown in Fig.9. In that case, increasing the parameter h increases the voltage and power responses, but still increases the displacement response. In all cases, increasing h slightly decreases the resonance frequency. It is worth noting that in this example, varying h was done easily by simply moving the control points in the present IGA framework. Note that for geometries like holes, multiple patches with C^1 continuity could be used, as described in [65].

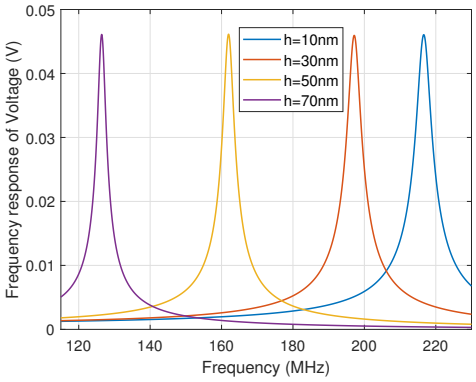

(a) Voltage frequency response

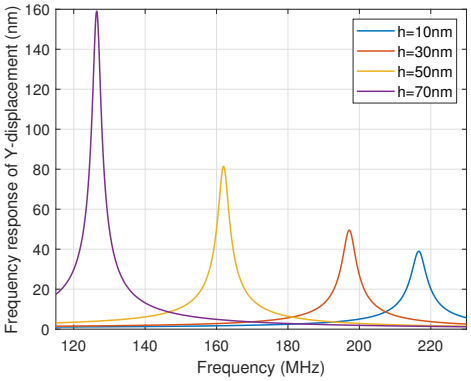

(b) y-displacement frequency response

Fig. 7: (a) Voltage and (b) displacement frequency responses with respect to the geometrical h parameter in the open-circuit conditions.

5.4 $h-p$ refinement effects on flexoelectric beam with complicated geometry

In this example, we investigate the effects of mesh refinement ($h-$refinement) and high-order approximation ($p-$refinement) of IGA to the dynamic analysis of flexoelectric structures with complex geometries, which could arise e.g. from CAD (Computer Aided Design). The geometry and boundary conditions of the beam

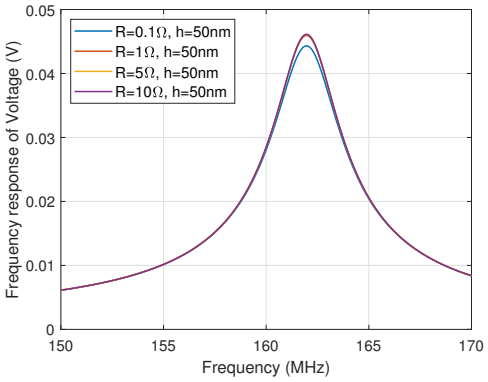

(a) Voltage frequency response

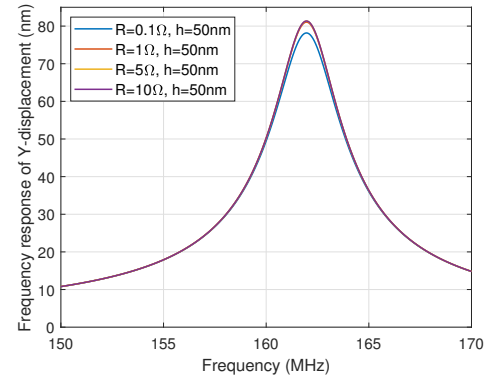

(b) y-displacement frequency response

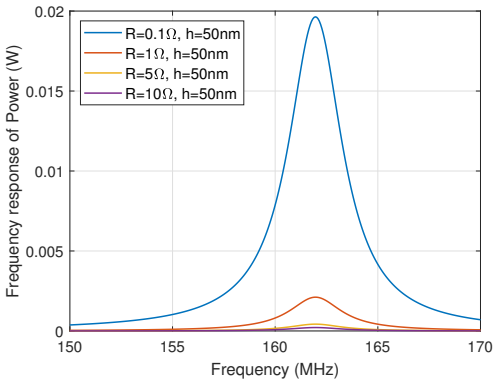

(c) Power frequency response

Fig. 8: (a) Voltage, (b) displacement and (c) power frequency responses with respect to resistor R for a fixed radius $h = 50$ nm in the close-circuit conditions.

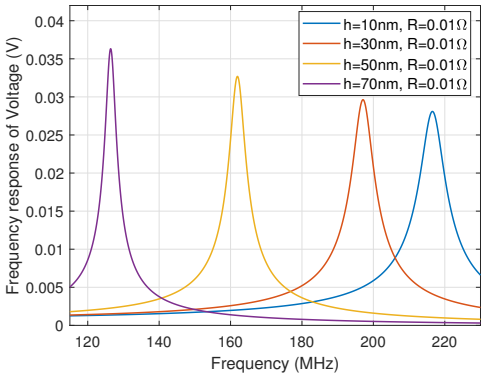

(a) Voltage frequency response

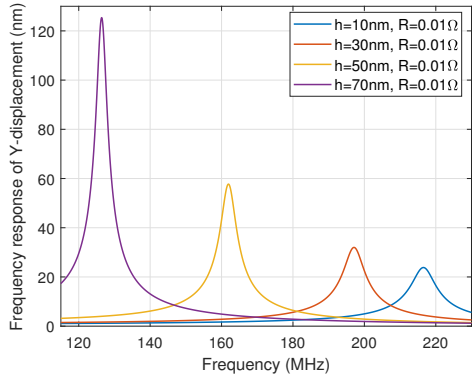

(b) y-displacement frequency response

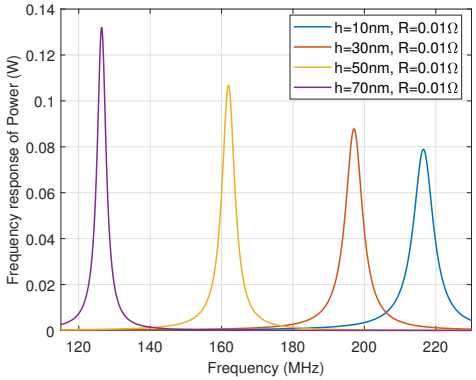

(c) Power frequency response

Fig. 9: Voltage and displacement and power frequency responses with respect to geometrical parameter h for resistor $R = 0.01\ \Omega$ in the close-circuit conditions

are shown in Fig.10. The geometric data, i.e. the control points defining the different NURBS curves, are provided in Table 3. The material parameters are listed in Appendix 8.

The maximum voltage frequency response is defined as the absolute value of voltage on the first resonance frequency at the top right corner of the structure. The convergence of the maximum voltage frequency response with respect to h and $p-$refinements is presented in Fig.11. We can appreciate the convergence of the solution using either h or p refinement. We can also observe from Fig. 11a that increasing the order of approximation p may be advantageous to quickly reach convergence, as compared to mesh refinement, which converges more slowly (see Fig. 11a.b). This constitutes an advantage over classical FEM, as increasing the order in FEM, especially considering C^1 continuity, introduces an intractable complexity. We can note from Fig.11a that the curves do not show an obvious convergence with respect to the mesh refinement, even though the differences between the response values for the different meshes are small. To extract the maximum voltage frequency response, it is required to solve the problem for different frequencies, and then interpolate to find the maximum value. We believe that this process might induce additional errors that could explain this low convergence with respect to the mesh.

6 Conclusions

In this work, we developed an isogeometric analysis (IGA) framework to solve the dynamic response of flexoelectric energy harvesters for arbitrary geometries,

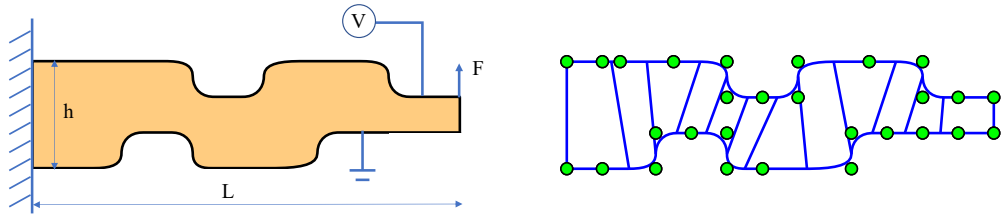

Fig. 10: Flexoelectric beam with complex geometry: (a) geometry and boundary conditions; (b) initial IGA discretization.

in the frequency domain, including strain gradient inertial effects. As compared to the previous related works available in the literature, the IGA discretization was proposed here for the first time to solve dynamic flexoelectric problems in the frequency domain. The conditions of both open and close-circuits were formulated. The potential of the present formulation has been applied to evaluate the sensitivity of different parameters such as load resistors, flexoelectricity, dynamic scale parameter and geometric features on the frequency response of output voltage, power and displacements of beam-like dynamic energy harvesters, possibly including structural geometrical features. It was shown that using a flexoelectric material instead of a piezoelectric material has a critical influence on the voltage response of the energy harvester in open circuit conditions, showing the optimal resistive loads in the close-circuits. We also observe that the dynamic length parameter related to the gradient inertial term has only a small influence on the numerical results. Then, we could conclude that creating large holes in a beam-like structure made of a flexoelectric material can significantly increase voltage, power

i	$B_{i,1}(\times 10nm)$	$w_{i,1}$	$B_{i,2}(\times 10nm)$	$w_{i,2}$
1	(0,0)	1	(0,6)	1
2	(2,0)	1	(2,6)	1
3	(5,0)	1	(3,6)	1
4	(5,2)	$1/\sqrt{2}$	(6,6)	1
5	(7,2)	1	(9,6)	1
6	(9,2)	$1/\sqrt{2}$	(9,4)	$1/\sqrt{2}$
7	(9,0)	1	(11,4)	1
8	(11,0)	1	(13,4)	$1/\sqrt{2}$
9	(16,0)	1	(13,6)	1
10	(16,2)	$1/\sqrt{2}$	(17,6)	1
11	(18,2)	1	(20,6)	1
12	(20,2)	1	(20,4)	$1/\sqrt{2}$
13	(22,2)	1	(22,4)	1
14	(24,2)	1	(24,4)	1

Table 3: Control points $B_{i,j}$ and weights $w_{i,j}$ for the geometry shown in Fig.10

and displacement responses in a dynamic energy harvester. Finally, the advantages of IGA for $h-$ and p-refinement in the present flexoelectric context with applications to dynamic loads have been demonstrated for complex geometries.

7 Acknowledgments

Xing Chen acknowledges the support from China Scholarship Council (CSC No. 202106370116)

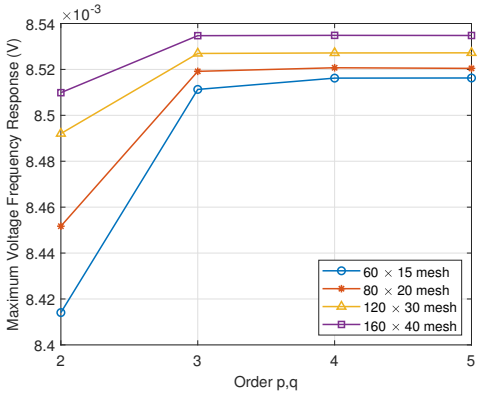

(a)

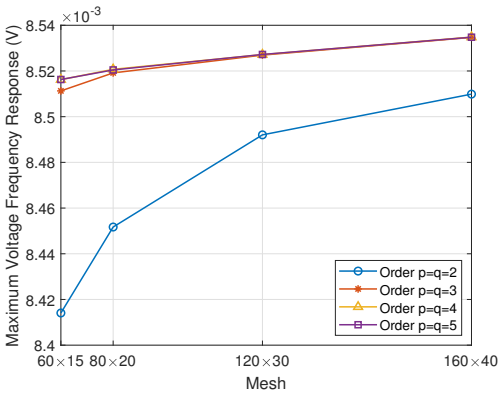

(b)

Fig. 11: Voltage frequency response on the first resonance with respect to (a) *h*-refinements and (b) $p-$refinement for open-circuit conditions.

8 Appendix: numerical values of material matrices

$$\mathbf{C}_1 = \begin{bmatrix} 132.1 & 84 & 0 \\ 84 & 155.6 & 0 \\ 0 & 0 & 35.8 \end{bmatrix} (GPa) \tag{76}$$

$$\boldsymbol{\mu} = \begin{bmatrix} 1.365 & 1.365 & 0 & 0 & 0 & 0 \\ 0 & 0 & 0 & 2.641 & 2.641 & 0 \end{bmatrix} (\times 10^{-4} C \cdot m^{-1}) \tag{77}$$

$$\boldsymbol{e} = \begin{bmatrix} -0.5217 & -0.5217 & 0 \\ 0 & 0 & 0 \end{bmatrix} (C \cdot m^{-2}) \tag{78}$$

$$\boldsymbol{\alpha}_1 = \begin{bmatrix} 2.102 & 0 \\ 0 & 4.065 \end{bmatrix} (nC^2 \cdot N^{-1} \cdot m^{-2}) \tag{79}$$

$$\mathbf{g} = \ell^2 \begin{bmatrix} 132.1 & 0 & 0 & 84 & 0 & 0 \\ 0 & 132.1 & 84 & 0 & 0 & 0 \\ 0 & 84 & 132.1 & 0 & 0 & 0 \\ 84 & 0 & 0 & 132.1 & 0 & 0 \\ 0 & 0 & 0 & 0 & 35.8 & 0 \\ 0 & 0 & 0 & 0 & 0 & 35.8 \end{bmatrix} \times 10^9 \tag{80}$$

References

1. J.K. Han, D.H. Jeon, S.Y. Cho, S.W. Kang, S.A. Yang, S.D. Bu, S. Myung, J. Lim, M. Choi, M. Lee, et al. Nanogenerators consisting of direct-grown piezoelectrics on multi-walled carbon nanotubes using flexoelectric effects. *Scientific reports*, 6(1):1–8, 2016.
2. Q. Deng, M. Kammoun, A. Erturk, and P. Sharma. Nanoscale flexoelectric energy harvesting. *International Journal of Solids and Structures*, 51(18):3218–3225, 2014.

3. X. Liang, S. Hu, and S. Shen. Nanoscale mechanical energy harvesting using piezoelectricity and flexoelectricity. *Smart Materials and Structures*, 26(3):035050, 2017.
4. A.D. Rey, P. Servio, and E.E. Herrera-Valencia. Stress-sensor device based on flexoelectric liquid crystalline membranes. *ChemPhysChem*, 15(7):1405–1412, 2014.
5. E.E. Herrera-Valencia and A.D. Rey. Actuation of flexoelectric membranes in viscoelastic fluids with applications to outer hair cells. *Philosophical Transactions of the Royal Society A: Mathematical, Physical and Engineering Sciences*, 372(2029):20130369, 2014.
6. V.S. Mashkevich and K.B. Tolpygo. Electrical, optical and elastic properties of diamond type crystals. *Soviet Physics JETP*, 5(3), Oct 1957.
7. P. Harris. Mechanism for the shock polarization of dielectrics. *Journal of Applied Physics*, 36(3):739–741, 1965.
8. W. Ma and L.E. Cross. Large flexoelectric polarization in ceramic lead magnesium niobate. *Applied Physics Letters*, 79(26):4420–4422, 2001.
9. W. Ma and L.E. Cross. Flexoelectric polarization of barium strontium titanate in the paraelectric state. *Applied Physics Letters*, 81(18):3440–3442, 2002.
10. S.M. Kogan. Piezoelectric effect during inhomogeneous deformation and acoustic scattering of carriers in crystals. *Soviet Physics-Solid State*, 5:197 – 224, 1964.
11. R. Maranganti, N.D. Sharma, and P. Sharma. Electromechanical coupling in nonpiezoelectric materials due to nanoscale nonlocal size effects: Green's function solutions and embedded inclusions. *Physical Review B*, 74(1):014110, 2006.
12. N.N. Sharma, R. Maranganti, and P. Sharma. On the possibility of piezoelectric nanocomposites without using piezoelectric materials. *Journal of the Mechanics and Physics of Solids*, 55(11):2328–2350, 2007.
13. W. Zhu, J.Y. Fu, N. Li, and L.E. Cross. Piezoelectric composite based on the enhanced flexoelectric effects. *Applied Physics Letters*, 89(19):192904, 2006.

14. S. Shen and S. Hu. A theory of flexoelectricity with surface effect for elastic dielectrics. *Journal of the Mechanics and Physics of Solids*, 58(5):665–677, 2010.

15. Q. Deng and S. Shen. The flexodynamic effect on nanoscale flexoelectric energy harvesting: a computational approach. *Smart Materials and Structures*, 27(10):105001, sep 2018.

16. S. Baroudi, F. Najar, and A. Jemai. Static and dynamic analytical coupled field analysis of piezoelectric flexoelectric nanobeams: a strain gradient theory approach. *International Journal of Solids and Structures*, 135:110–124, 2018.

17. K.F. Wang and B.L. Wang. An analytical model for nanoscale unimorph piezoelectric energy harvesters with flexoelectric effect. *Composite Structures*, 153:253–261, 2016.

18. S.D. Hu, H. Li, and H. Tzou. Sensing signal and energy generation analysis on a flexoelectric beam. In *ASME International Mechanical Engineering Congress and Exposition*, volume 45226, pages 523–531. American Society of Mechanical Engineers, 2012.

19. M. Fan, B. Deng, and H. Tzou. Dynamic flexoelectric actuation and vibration control of beams. *Journal of Vibration and Acoustics*, 140(4), 2018.

20. X. Zhang, H. Li, and H. Tzou. Analytical and experimental studies of flexoelectric beam control. In *ASME International Mechanical Engineering Congress and Exposition*, volume 50558, page V04BT05A054. American Society of Mechanical Engineers, 2016.

21. Z. Yan. Modeling of a nanoscale flexoelectric energy harvester with surface effects. *Physica E: Low-dimensional Systems and Nanostructures*, 88:125–132, 2017.

22. Z. Yan and L. Jiang. Size-dependent bending and vibration behaviour of piezoelectric nanobeams due to flexoelectricity. *Journal of Physics D: Applied Physics*, 46(35):355502, aug 2013.

23. D.P. Zhang, Y.J. Lei, and S. Adhikari. Flexoelectric effect on vibration responses of piezoelectric nanobeams embedded in viscoelastic medium based on nonlocal elasticity theory. *Acta Mechanica*, 229(6):2379–2392, 2018.
24. B.H. Nguyen, S.S. Nanthakumar, X. Zhuang, P. Wriggers, X. Jiang, and T. Rabczuk. Dynamic flexoelectric effect on piezoelectric nanostructures. *European Journal of Mechanics - A/Solids*, 71:404–409, 2018.
25. P. Yu, W. Leng, L. Peng, Y. Suo, and J. Guo. The bending and vibration responses of functionally graded piezoelectric nanobeams with dynamic flexoelectric effect. *Results in Physics*, 28:104624, 2021.
26. Z. Zhang, Z. Yan, and L. Jiang. Flexoelectric effect on the electroelastic responses and vibrational behaviors of a piezoelectric nanoplate. *Journal of Applied Physics*, 116(1):014307, 2014.
27. K.B. Shingare and S.I. Kundalwal. Static and dynamic response of graphene nanocomposite plates with flexoelectric effect. *Mechanics of Materials*, 134:69–84, 2019.
28. K.F. Wang and B.L. Wang. Non-linear flexoelectricity in energy harvesting. *International Journal of Engineering Science*, 116:88–103, 2017.
29. S. Baroudi and F. Najar. Dynamic analysis of a nonlinear nanobeam with flexoelectric actuation. *Journal of Applied Physics*, 125(4):044503, 2019.
30. M. Zarepour, S.A.H. Hosseini, and A.H. Akbarzadeh. Geometrically nonlinear analysis of timoshenko piezoelectric nanobeams with flexoelectricity effect based on eringen's differential model. *Applied Mathematical Modelling*, 69:563–582, 2019.
31. M. Ajri, A. Rastgoo, and M.M.S. Fakhrabadi. How does flexoelectricity affect static bending and nonlinear dynamic response of nanoscale lipid bilayers? *Physica Scripta*, 95(2):025001, 2019.
32. L. Chen, S. Pan, Y. Fei, W. Zhang, and F. Yang. Theoretical study of micro/nanoscale bistable plate for flexoelectric energy harvesting. *Applied Physics A*, 125(4):1–11,

2019.

33. A. Abdollahi, C. Peco, D. Millán, M. Arroyo, and I. Arias. Computational evaluation of the flexoelectric effect in dielectric solids. *Journal of Applied Physics*, 116(9):093502, 2014.
34. A. Abdollahi, D. Millán, C. Peco, M. Arroyo, and I. Arias. Revisiting pyramid compression to quantify flexoelectricity: A three-dimensional simulation study. *Physical Review B*, 91:104103, Mar 2015.
35. S. Mao, P.K. Purohit, and N. Aravas. Mixed finite-element formulations in piezoelectricity and flexoelectricity. *Proceedings of the Royal Society A: Mathematical, Physical and Engineering Sciences*, 472(2190):20150879, 2016.
36. F. Deng, Q. Deng, W. Yu, and S. Shen. Mixed finite elements for flexoelectric solids. *Journal of Applied Mechanics*, 84(8), 2017.
37. H. Ghasemi, H.S. Park, and T. Rabczukk. A level-set based iga formulation for topology optimization of flexoelectric materials. *Computer Methods in Applied Mechanics and Engineering*, 313:239 – 258, 2017.
38. T.Q. Thai, T. Rabczuk, and X. Zhuang. A large deformation isogeometric approach for flexoelectricity and soft materials. *Computer Methods in Applied Mechanics and Engineering*, 341:718–739, 2018.
39. B.H. Nguyen, X. Zhuang, and T. Rabczuk. Numerical model for the characterization of maxwell-wagner relaxation in piezoelectric and flexoelectric composite material. *Computers & Structures*, 208:75–91, 2018.
40. D. Codony, O. Marco, S. Fernández-Méndez, and I. Arias. An immersed boundary hierarchical b-spline method for flexoelectricity. *Computer Methods in Applied Mechanics and Engineering*, 354:750–782, 2019.
41. J. Yvonnet and L.P. Liu. A numerical framework for modeling flexoelectricity and maxwell stress in soft dielectrics at finite strains. *Computer Methods in Applied Me-*

chanics and Engineering, 313:450 – 482, 2017.

42. A. Kumar, A. Sharma, R. Kumar, R. Vaish, and V.S. Chauhan. Finite element analysis of vibration energy harvesting using lead-free piezoelectric materials: A comparative study. *Journal of Asian Ceramic Societies*, 2(2):138–143, 2014.
43. A. Kumar, A. Sharma, R. Vaish, R. Kumar, and S.C. Jain. A numerical study on flexoelectric bistable energy harvester. *Applied Physics A*, 124(7):1–9, 2018.
44. T.Q. Thai, X. Zhuang, H.S. Park, and T. Rabczuk. A staggered explicit-implicit isogeometric formulation for large deformation flexoelectricity. *Engineering Analysis with Boundary Elements*, 122:1–12, 2021.
45. J. Xue, L. Chen, L. Chang, and W. Zhang. A wideband flexoelectric energy harvester based on graphene substrate. *Engineering Structures*, 231:111779, 2021.
46. S. Papargyri-Beskou, D. Polyzos, and D.E. Beskos. Wave dispersion in gradient elastic solids and structures: A unified treatment. *International Journal of Solids and Structures*, 46(21):3751–3759, 2009.
47. P.A. Gourgiotis, H.G. Georgiadis, and I. Neocleous. On the reflection of waves in half-spaces of microstructured materials governed by dipolar gradient elasticity. *Wave Motion*, 50(3):437–455, 2013.
48. Y. Li and P. Wei. Reflection and transmission through a microstructured slab sandwiched by two half-spaces. *European Journal of Mechanics - A/Solids*, 57:1–17, 2016.
49. J. Sladek, V. Sladek, M.v Repka, and Q. Deng. Flexoelectric effect in dielectrics under a dynamic load. *Composite Structures*, 260:113528, 2021.
50. H. Askes and E.C. Aifantis. Gradient elasticity in statics and dynamics: An overview of formulations, length scale identification procedures, finite element implementations and new results. *International Journal of Solids and Structures*, 48(13):1962–1990, 2011.

51. J.Y. Fu, W. Zhu, N. Li, and L.E. Cross. Experimental studies of the converse flexoelectric effect induced by inhomogeneous electric field in a barium strontium titanate composition. *Journal of Applied Physics*, 100(2):024112, 2006.

52. X. Chen, J. Yvonnet, H.S. Park, and S. Yao. Enhanced converse flexoelectricity in piezoelectric composites by coupling topology optimization with homogenization. *Journal of Applied Physics*, 129(24):245104, 2021.

53. R. Maranganti and P. Sharma. A novel atomistic approach to determine strain-gradient elasticity constants: Tabulation and comparison for various metals, semiconductors, silica, polymers and the (ir) relevance for nanotechnologies. *Journal of the Mechanics and Physics of Solids*, 55(9):1823–1852, 2007.

54. T.J.R. Hughes, J.A. Cottrell, and Y. Bazilevs. Isogeometric analysis: Cad, finite elements, nurbs, exact geometry and mesh refinement. *Computer Methods in Applied Mechanics and Engineering*, 194(39):4135–4195, 2005.

55. V.P. Nguyen and S. Bordas. *Extended Isogeometric Analysis for Strong and Weak Discontinuities*, pages 21–120. Springer Vienna, Vienna, 2015.

56. D.B. Carl. *A practical guide to splines*, volume 27. springer-verlag New York, 1978.

57. J. Yvonnet, X. Chen, and P. Sharma. Apparent flexoelectricity due to heterogeneous piezoelectricity. *Journal of Applied Mechanics*, 87(11):111003, 2020.

58. S.S. Nanthakumar, X. Zhuang, H.S. Park, and T. Rabczuk. Topology optimization of flexoelectric structures. *Journal of the Mechanics and Physics of Solids*, 105:217 – 234, 2017.

59. M.S. Majdoub, P. Sharma, and T. Çağin. Erratum: Enhanced size-dependent piezoelectricity and elasticity in nanostructures due to the flexoelectric effect. *Physical Review B*, 79:119904, Mar 2009.

60. M. Fan and H. Tzou. Vibration control with the converse flexoelectric effect on the laminated beams. *Journal of Intelligent Material Systems and Structures*, 30(17):2556–

2566, 2019.

61. X. Chen, J. Yvonnet, S. Yao, and H.S. Park. Topology optimization of flexoelectric composites using computational homogenization. *Computer Methods in Applied Mechanics and Engineering*, 381:113819, 2021.
62. I.M. Gitman, H. Askes, E. Kuhl, and E.C. Aifantis. Stress concentrations in fractured compact bone simulated with a special class of anisotropic gradient elasticity. *International Journal of Solids and Structures*, 47(9):1099–1107, 2010.
63. L. Wang and H. Hu. Flexural wave propagation in single-walled carbon nanotubes. *Physical Review B*, 71:195412, May 2005.
64. C.A. Felippa. Introduction to finite element methods. *University of Colorado*, 885, 2004.
65. C.L. Chan, C. Anitescu, and T. Rabczuk. Isogeometric analysis with strong multipatch c1-coupling. *Computer Aided Geometric Design*, 62:294–310, 2018.